Advances in Nano Research, *Vol. 19, No. 1 (2025) 13-27*
https://doi.org/10.12989/anr.2025.19.1.013

Assessing thermomechanical stability characteristics of shear deformable sandwich composite toroidal shells with bio-inspired auxetic core

Mohammadhossein Goudarzfallahi[1], Farzad Ebrahimi*[2] and Ali Alinia Ziazi[1]

[1]*Department of Mechanical Engineering, SR.C., Islamic Azad University, Tehran, Iran*
[2]*Department of Mechanical Engineering, Faculty of Engineering, Imam Khomeini International University, Qazvin, Iran*

(*Received January 6, 2025, Revised May 28, 2025, Accepted June 19, 2025*)

Abstract. This work investigates the thermomechanical stability response of bio-inspired auxetic-core, shear-deformable sandwich toroidal shell segments (TSSs) with carbon nanotube (CNT)-reinforced face sheets. The TSSs are subjected to external pressure and thermal fields, including a uniform temperature rise and linear or nonlinear gradients along the shell thickness, and are supported by a Kerr foundation. The core of the sandwich structure features an innovative auxetic metamaterial modeled after the geometry of a butterfly, known as a butterfly-shaped auxetic design. This proposed topological design offers greater stiffness than conventional re-entrant auxetic structures with a negative Poisson's ratio (NPR). The fundamental equations are established within the framework of Reddy's third-order shear deformation theory (TSDT), and the Galerkin method is employed to obtain the nonlinear postbuckling response of the sandwich shells. Comparison with prior studies verifies the accuracy of the proposed model. Numerical analyses reveal the influence of the butterfly-shaped auxetic core's geometric parameters, thermal conditions, and Kerr foundation properties on critical buckling loads and postbuckling curves. Results demonstrate the proposed auxetic core's superior stability to traditional re-entrant auxetic structures, providing valuable insights for designing lightweight metamaterial TSSs with NPR for advanced engineering applications.

Keywords: arc-type auxetic metamaterial core; carbon nanotubes; Kerr foundation; porosity; stability; toroidal shell segment; TSDT

1. Introduction

The emergence of advanced metamaterials and engineering methods has facilitated the investigation of new-generation structures with unconventional characteristics. Among these, auxetic materials, which are known for their negative Poisson's ratio (NPR), have become an interesting area of research. The field was revolutionized in 1987 when Lakes introduced auxetic foam, showing that NPR behavior could be achieved through precise microstructural design, such as inverted cell shapes (Lakes 1987). This breakthrough sparked considerable interest in designing auxetic structures with beneficial mechanical behaviors, including enhanced shear and indentation resistance, superior energy absorption, improved crashworthiness, and greater fracture toughness. These characteristics have consequently facilitated their use in aerospace, biomedical engineering, sensors, and advanced civil engineering structures (Ebrahimi 2024). Recent developments have focused on integrating auxetic cores into sandwich-structured composites, resulting in advanced materials with significantly improved static and dynamic load-bearing capabilities. For example, Ebrahimi and Dadashi (2023) examined the vibration response of cylindrical shells featuring auxetic cores subjected to axial loading and external disturbances. Li and Liu (2022) focused on the thermal buckling of sandwich shells incorporating a honeycomb core with tunable mechanical characteristics. Significant progress has been made in engineering advanced auxetic materials with enhanced mechanical performance by leveraging their unique deformation behavior to achieve both auxeticity and high stiffness. Drawing from Miura- and graphene-origami (GOri) frameworks, Zhao *et al.* (2022a) developed GOri-based metallic metamaterials (GOEAMs) exhibiting adjustable NPR and improved mechanical attributes. Subsequent efforts addressed the dynamic behavior, free vibration (Zhao *et al.* 2022b), and buckling/postbuckling responses (Zhao *et al.* 2022c) of GOEAM beams, confirming their potential for tunable stability in structural applications. The buckling of composite nanoplates composed of GOEAM was studied by Ebrahimi and Ahari (2024). Ghafouri *et al.* (2023) investigated sound transmission loss (STL) of sandwich shells employing 3D re-entrant cores. By introducing a star-shaped auxetic core, Yu *et al.* (2024) revealed enhanced STL performance in sandwich panels compared to conventional NPR designs. Furthermore, Li *et al.* (2022) assessed the impact response of sandwich cylindrical shells containing double-V auxetic structures. Fu *et al.* (2024) explored the impact performance of sandwich shells featuring arc-type auxetic cores. Recent developments also highlight the promise of auxetic metamaterials inspired by biological patterns, such as butterfly-shaped structures. For instance, Wang and Fu (2024) showed that sandwich plates with auxetic butterfly cores have greater stiffness and STL than those with re-entrant cores.

Carbon nanotubes (CNTs) significantly enhance

*Corresponding author, Ph.D., Professor,
E-mail: febrahimy@eng.ikiu.ac.ir

ISSN: 2287-237X (Print), 2287-2388 (Online)

composite structures due to their outstanding thermal, mechanical, and electrical properties. As reinforcing fibers, CNTs can be distributed in a polymer matrix uniformly (UD) or functionally graded (FG) (Ebrahimi and Dabbagh, 2020). Shen (2011a, b) analyzed the postbuckling behavior of FG-CNTRC cylindrical shells. Duc *et al*. (2020) studied the nonlinear buckling of CNTRC imperfect cylindrical panels. Ebrahimi and Dabbagh (2023) examined the influence of porosity on CNT-reinforced meta-nano-composites. Zhao *et al*. (2024) conducted a buckling analysis of CNTRC conical shells. Shen and Xiang (2013) investigated the postbuckling behavior of CNTRC cylindrical shells under external pressure in a thermal environment. In their study, Chakraborty and Dey (2023) evaluated the stability of CNTRC sandwich panels with CNT-reinforced coatings and a soft core. Hieu and Van Tung (2020a) explored the thermomechanical postbuckling of CNTRC cylindrical shells under varying thermal loads, followed by a study on their stability under uniform temperature rise (Hieu and Van Tung 2021). Van Quyen *et al*. (2021) analyzed the nonlinear vibration of sandwich composite cylindrical panels with auxetic honeycomb cores and CNTRC face sheets under blast loading and thermal effects.

Graphene is emerging as a next-generation reinforcement material for polymer matrices. Recent studies have increasingly focused on graphene platelet (GPL)-reinforced composite shells due to their exceptional mechanical and functional properties. Discovered in 2004, graphene has attracted significant interest from researchers because of its two-dimensional nanostructure, exceptional mechanical strength, and outstanding thermal and electrical conductivity. These attributes make it a promising candidate for enhancing the performance of conventional materials. For instance, Chen *et al*. (2020) investigated the free vibration and transient response of FGP-GPLRC cylindrical shells resting on elastic foundations. Similarly, Qin *et al*. (2020) conducted a free vibration analysis of FGP-GPLRC cylindrical shells embedded in elastic foundations, considering porosity effects. Nguyen *et al*. (2023) analyzed the free vibration behavior of FG-GPLRC spherical shell segments.

Toroidal shell segments (TSSs) are commonly utilized in various engineering fields, such as aerospace, marine, and civil structures. Structural modifications can be achieved by varying the curvature radius. Nguyen *et al*. (2022) investigated the free vibration of rotating stiffened FG-GPLRC TSSs in thermal environments. In a similar study, Nguyen *et al*. (2023a) extended the analysis to include varying boundary conditions. Significant attention has been devoted to examining the static and dynamic stability of TSSs. Stein and McElman (1965), employing classical shell theory (CST), analyzed the buckling of TSSs under external pressure. Hutchinson (1967) used CST to investigate the early postbuckling behavior of TSSs under multiple loading scenarios. Building on CST and the approximation proposed by Stein and McElman (1965), Phuong *et al*. (2021) explored the nonlinear buckling and postbuckling response of GRC TSSs subjected to radial loads and thermal fields and supported by elastic foundations. More recently, several studies have extended this framework to enhance stability using nanocomposites and auxetic cores (Van Tien *et al*. 2022, Ebrahimi *et al*. 2024a, b, Nguyen *et al*. 2023, Nam *et al*. 2022, Phuong *et al*. 2023, Hoai Nam *et al*. 2024), Van Tien *et al*. (2022) examined nonlinear buckling in sandwich TSSs with a honeycomb auxetic core and CNT-reinforced coatings. More recently, several studies have focused on enhancing the stability performance of sandwich TSSs using the GOREAM core. Ebrahimi *et al*. (2024a) evaluated its performance, showing enhanced stability over conventional re-entrant auxetic designs under external radial pressure. The effect of axial compression was addressed in Ebrahimi *et al*. (2025a), while combined loading conditions were investigated by Ebrahimi *et al*. (2024b). Porosity effects on the structural response were explored in Ebrahimi *et al*. (2024c), and the influence of stiffeners on stability was studied in Ebrahimi *et al*. (2025d). The introduction of an arc-type auxetic core was examined in Ebrahimi *et al*. (2024d). Additionally, a bio-inspired auxetic configuration was proposed by Ebrahimi *et al*. (2025a), and Ebrahimi *et al*. (2025c) further investigated various auxetic core types and analyzed the nonlinear stability of sandwich TSSs with CNT-reinforced face sheets.

A review of the literature reveals that no previous studies have investigated the thermomechanical stability of sandwich TSSs with auxetic cores using shear-deformable theories under external pressure. Prior works mostly focus on thin shells and often overlook the effects of shear deformation, which is an important aspect for accurately capturing the nonlinear postbuckling behavior of moderately thick shells. Although thermal loading plays a critical role in the stability of these structures, its effects remain insufficiently studied, which calls for an in-depth investigation. In addition, newly developed auxetic metamaterials, with advanced topologies and enhanced mechanical behavior, have received little attention in existing stability analyses.

To address these limitations, the authors develop an analytical method to examine the thermomechanical behavior of shear-deformable sandwich TSSs under external pressure and thermal loading supported by a Kerr elastic foundation utilizing TSDT. The sandwich structure incorporates a newly developed bio-inspired auxetic core—the butterfly-shaped auxetic metamaterial—which modifies the conventional re-entrant design to enhance in-plane stiffness while retaining NPR behavior. Its bio-inspired geometry offers greater adaptability to complex shapes and loading conditions. The practical feasibility of this meta-material was also demonstrated by Yifeng *et al*. (2025) recently, who designed 3D-printed butterfly-shaped auxetic specimens, confirming its applicability. This structure offers higher stiffness, contributing to improved buckling and postbuckling performance and making it especially suitable for lightweight sandwich structures in demanding fields such as aerospace and space engineering. Another novelty of this study is the analysis of different types of thermal loading to reflect practical situations with varying temperature conditions. Additionally, the Kerr foundation models the interaction between sandwich shells and elastic media by accounting for both shear and normal stiffness, which allows for a more accurate representation of support

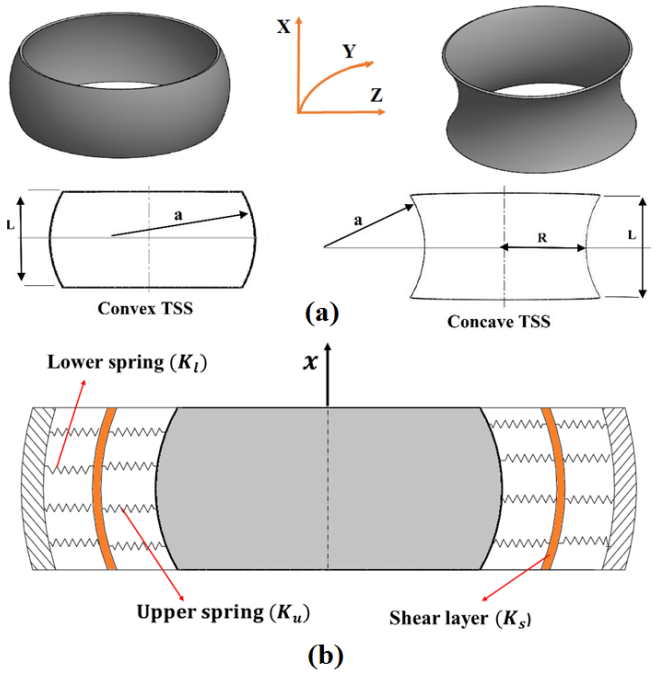

Fig. 1 Schematic of TSSs supported by a Kerr foundation

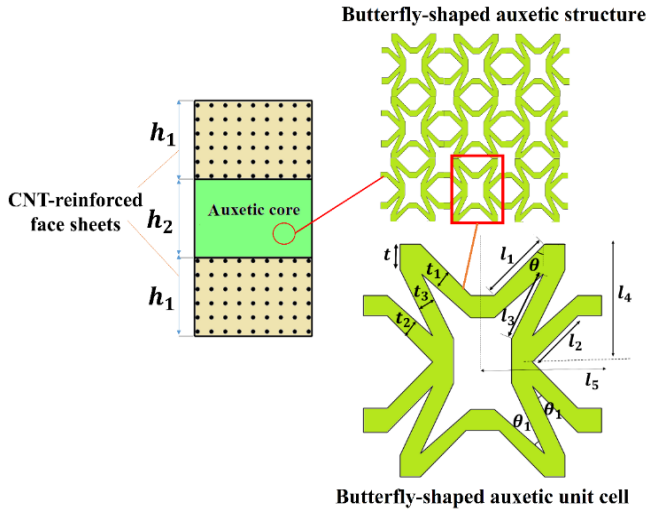

Fig. 2 Schematic of an auxetic-core sandwich structure

conditions in civil, mechanical, and marine engineering. This work is expected to provide an extensive reference for designing and utilizing novel auxetic-core sandwich shell structures to enhance their structural stability.

2. Structural configuration and material characteristics

2.1 Geometric modeling

Fig. 1 depicts TSSs with length L, thickness h, and principal radii of middle surface a and R in the meridional and circumferential directions. A coordinate system (x, y, z) is established with the origin positioned at the middle surface and edge of the shell, where x, y, and z denote the longitudinal, circumferential, and radial directions, respectively. The Kerr foundation supports the entire TSS, which is represented as two springs linked by a shear layer.

A schematic of the sandwich composite structure is illustrated in Fig. 2, featuring an auxetic core with a thickness of h_2 and external CNT-reinforced face sheets of thickness h_1.

2.2 Material characteristics

2.2.1 The bio-inspired auxetic core

The core of the sandwich composite in this study is butterfly-shaped auxetic (Fig. 2), with elastic moduli given as (Ebrahimi *et al*. 2025c):

$$
\begin{aligned}
E_1^c &= \frac{E_s}{\alpha_1[(\mu^3-\mu)\cos^2\alpha+2+\mu]}\\
E_2^c &= \frac{E_s\alpha_1}{(\mu^3-\mu)\sin^2\alpha+2+\mu}\\
G_{12}^c &= \frac{E_s l_4 l_5}{2l_4^2\kappa(\cos^2\theta+\kappa^2\sin^2\theta)+r}\\
G_{13}^c &= G_{23}^c = G_s\frac{(2cos\theta+cos\alpha)^2}{l_4 l_5(2\kappa+\mu)}\\
\nu_{12}^c &= -\frac{(\mu^3-\mu)\sin(2\alpha)}{2\alpha_1[\mu+2+(\mu^3-\mu)\cos^2\alpha]}\\
\nu_{21}^c &= -\frac{\alpha_1(\mu^3-\mu)\sin(2\alpha)}{2[\mu+2+(\mu^3-\mu)\sin^2\alpha]}
\end{aligned}
\tag{1}
$$

where the geometric parameters of the unit cell are given as follows (Ebrahimi *et al*. 2025c):

$$
\begin{aligned}
r &= \mu(l_5 sin\alpha - l_4 cos\alpha)^2+\mu^3(l_4 sin\alpha+l_5 cos\alpha)^2,\\
&\alpha_1 = l_4/l_5,\ \alpha=\theta-\theta_1\\
l_4 &= 2t+l_3\cos\alpha,\ l_5 = 3t+2l_1\sin\theta-l_3\sin\alpha,\\
&\kappa = l_1/t_1,\ \alpha=\theta-\theta_1,\\
&\alpha_1 = l_4/l_5\ \ t_1=t_2=t\sin\theta,\ \mu=l_3/t_3
\end{aligned}
\tag{2}
$$

2.2.2 The CNT-reinforced face sheets

The volume fractions of CNT for the external face sheets are defined as follows (Shen 2011a, b):

$$
\begin{aligned}
V_{CNT} &= \bar{V}_{CNT}\ (\mathrm{UD})\\
V_{CNT} &= \left(\frac{4|z|}{h_1}\right)\bar{V}_{CNT}\ (\mathrm{FG-X})\\
V_{CNT} &= \left(2-\frac{4|z|}{h_1}\right)\bar{V}_{CNT}\ (\mathrm{FG-O})
\end{aligned}
\tag{3}
$$

The orthotropic moduli of the CNT-reinforced face sheets are calculated considering the extended rule of mixtures (Shen 2011a, b) as follows:

$$
\begin{aligned}
E_{11}^{CNTRC} &= V_{ma}E_{ma}+\eta_1 V_{CNT}E_{11}^{CNT},\\
E_{22}^{CNTRC} &= \eta_2\Big/\left(\frac{V_{CNT}}{E_{22}^{CNT}}+\frac{V_{ma}}{E_{ma}}\right)\\
G_{12}^{CNTRC} &= \eta_3\Big/\left(\frac{V_{CNT}}{G_{12}^{CNT}}+\frac{V_{ma}}{G_{ma}}\right),\\
\nu_{12}^{CNTRC} &= V_{ma}\nu_{ma}+V_{CNT}\nu_{12}^{CNT}
\end{aligned}
\tag{4}
$$

where E_{11}^{CNT} and E_{22}^{CNT} are the elastic moduli, and G_{12}^{CNT} and ν_{12}^{CNT}, denote the shear modulus and Poisson's ratio of the CNTs, while E_{ma}, G_{ma}, and ν_{ma} are the elastic moduli, shear moduli, and Poisson's ratios for the matrix. The efficiency parameters of the CNTs are indicated by η_j (j = 1, 2, 3). Additionally, the temperature-dependent properties are based on the results of Shen (2011a, b) and Shen and Xiang (2013).

3. Nonlinear equilibrium equations

The nonlinear equilibrium equations of TSSs are established using the TSDT. Accordingly, the displacement field at a distance z from the middle surface is as follows (Reddy and Liu 1987, Reddy 2003):

$$\begin{pmatrix}\bar{u}\\ \bar{v}\\ \bar{w}\end{pmatrix}=\begin{pmatrix}u+z\phi_x-\frac{4}{3h^2}z^3(\phi_x+\frac{\partial w_0}{\partial x})\\ v+z\phi_y-\frac{4}{3h^2}z^3(\phi_y+\frac{\partial w_0}{\partial y})\\ w\end{pmatrix} \tag{5}$$

where u, v, and w are displacements of the middle surface, and ϕ_x and ϕ_y denote the transverse-normal rotations about the *x* and *y* axes, respectively.

The strain components at a distance *z* from the middle surface of shells, including von Kármán nonlinear terms, are expressed as follows: (Reddy and Liu 1987, Reddy 2003):

$$\begin{pmatrix}\varepsilon_x\\ \varepsilon_y\\ \gamma_{xy}\end{pmatrix}=\begin{pmatrix}\varepsilon_x^0\\ \varepsilon_y^0\\ \gamma_{xy}^0\end{pmatrix}+z\begin{pmatrix}k_x^{(1)}\\ k_y^{(1)}\\ k_{xy}^{(1)}\end{pmatrix}+z^3\begin{pmatrix}k_x^{(3)}\\ k_y^{(3)}\\ k_{xy}^{(3)}\end{pmatrix}$$
$$\begin{pmatrix}\gamma_{xz}\\ \gamma_{yz}\end{pmatrix}=\begin{pmatrix}\gamma_{xz}^0\\ \gamma_{yz}^0\end{pmatrix}+z^2\begin{pmatrix}k_{xz}^{(2)}\\ k_{yz}^{(2)}\end{pmatrix} \tag{6}$$

where

$$\begin{pmatrix}\varepsilon_x^0\\ \varepsilon_y^0\\ \gamma_{xy}^0\end{pmatrix}=\begin{pmatrix}u_{,x}-w/a+w_{,x}^2/2\\ v_{,y}-w/R+w_{,y}^2/2\\ u_{,y}+v_{,x}+w_{,x}w_{,y}\end{pmatrix},\quad \begin{pmatrix}\gamma_{xz}^0\\ \gamma_{yz}^0\end{pmatrix}=\begin{pmatrix}\phi_x+w_{,x}\\ \phi_y+w_{,y}\end{pmatrix} \tag{7}$$

Furthermore:

$$\begin{pmatrix}k_x^{(1)}\\ k_y^{(1)}\\ k_{xy}^{(1)}\end{pmatrix}=\begin{pmatrix}\phi_{x,x}\\ \phi_{y,y}\\ \phi_{x,y}+\phi_{y,x}\end{pmatrix},\quad \begin{pmatrix}k_x^{(3)}\\ k_y^{(3)}\\ k_{xy}^{(3)}\end{pmatrix}=-c\begin{pmatrix}\phi_{x,x}+w_{,xx}\\ \phi_{y,y}+w_{,yy}\\ \phi_{x,y}+\phi_{y,x}+2w_{,xy}\end{pmatrix}$$
$$\begin{pmatrix}k_{xz}^{(2)}\\ k_{yz}^{(2)}\end{pmatrix}=-3c\begin{pmatrix}\phi_x+w_{,x}\\ \phi_y+w_{,y}\end{pmatrix}\quad c=4/3h^2 \tag{8}$$

Hooke's law accounting for temperature effects is expressed as:

$$\begin{Bmatrix}\sigma_x\\ \sigma_y\\ \sigma_{yz}\\ \sigma_{xz}\\ \sigma_{xy}\end{Bmatrix}=\begin{bmatrix}Q_{11}&Q_{12}&0&0&0\\ Q_{12}&Q_{22}&0&0&0\\ 0&0&Q_{55}&0&0\\ 0&0&0&Q_{44}&0\\ 0&0&0&0&Q_{66}\end{bmatrix}\left[\begin{Bmatrix}\varepsilon_x\\ \varepsilon_y\\ \gamma_{yz}\\ \gamma_{xz}\\ \gamma_{xy}\end{Bmatrix}-\Delta T\begin{Bmatrix}\alpha_{11}\\ \alpha_{22}\\ 0\\ 0\\ 0\end{Bmatrix}\right] \tag{9}$$

where

$$Q_{11}=\frac{E_{11}}{1-v_{12}v_{21}},\ Q_{12}=\frac{v_{21}E_{11}}{1-v_{12}v_{21}},\quad Q_{22}=\frac{E_{22}}{1-v_{12}v_{21}},\quad Q_{44}=G_{23},\quad Q_{55}=G_{13},\quad Q_{66}=G_{12} \tag{10}$$

The force and moment resultants of sandwich TSSs are defined as

$$(N_i,M_i,P_i)=\int_{-h/2}^{h/2}\sigma_i\,(1,z,z^3)dz,\quad i=x,y,xy$$
$$(Q_j,R_j)=\int_{-h/2}^{h/2}\sigma_{iz}\,(1,z^2)dz,\quad i=x,y \tag{11}$$

By substituting Eq. (6) into Eq. (9) and subsequently incorporating the resulting expression into Eq. (11), we obtain

$$\begin{aligned}
N_x&=A_{11}\epsilon_x^0+A_{12}\epsilon_y^0+A_{13}k_x+A_{14}k_y+A_{15}k_x^3\\
&\quad+A_{16}k_y^3-A_{17}\Phi_{,y}-\Psi_1\\
N_y&=A_{12}\epsilon_x^0+A_{22}\epsilon_y^0+A_{23}k_x+A_{24}k_y+A_{25}k_x^3\\
&\quad+A_{26}k_y^3-A_{27}\Phi_{,y}-\Psi_2\\
N_{xy}&=A_{31}\gamma_{xy}^0+A_{32}k_{xy}+A_{33}k_{xy}^3\\
M_x&=A_{13}\epsilon_x^0+A_{14}\epsilon_y^0+A_{43}k_x+A_{44}k_y+A_{45}k_x^3\\
&\quad+A_{46}k_y^3-\Psi_3\\
M_y&=A_{14}\epsilon_x^0+A_{24}\epsilon_y^0+A_{44}k_x+A_{54}k_y+A_{46}k_x^3\\
&\quad+A_{56}k_y^3-\Psi_4\\
M_{xy}&=A_{32}\gamma_{xy}^0+A_{62}k_{xy}+A_{63}k_{xy}^3\\
P_x&=A_{71}\epsilon_x^0+A_{16}\epsilon_y^0+A_{73}k_x+A_{46}k_y+A_{75}k_x^3\\
&\quad+A_{76}k_y^3-\Psi_5\\
P_y&=A_{16}\epsilon_x^0+A_{82}\epsilon_y^0+A_{46}k_x+A_{84}k_y+A_{76}k_x^3\\
&\quad+A_{86}k_y^3-\Psi_6\\
P_{xy}&=A_{33}\gamma_{xy}^0+A_{63}k_{xy}+A_{93}k_{xy}^3Q_x\\
&=A_{94}\gamma_{xy}^0+A_{95}k_{xz}^2\\
Q_y&=A_{96}\gamma_{xy}^0+A_{97}k_{yz}^2\\
K_x&=A_{98}\gamma_{xz}^0+A_{99}k_{xz}^2\\
K_y&=A_{100}\gamma_{xy}^0+A_{101}k_{yz}^2
\end{aligned} \tag{12}$$

Here, the coefficients A_{ij} and Ψ_i are determined, as

explained by Ebrahimi *et al*. (2024d, 2025c).

The nonlinear equilibrium equations for TSSs are expressed as follows (Ebrahimi *et al*. 2025c, Reddy 2003):

$$\begin{matrix} N_{x,x} + N_{xy,y} = 0 \\ N_{xy,x} + N_{y,y} = 0 \end{matrix} \tag{13}$$

$$\begin{matrix} Q_{x,x} + Q_{y,y} - 3c\left(R_{x,x} + R_{y,y}\right) \\ +c\left(P_{x,xx} + 2P_{xy,xy} + P_{y,yy}\right) + \frac{N_x}{a} + \frac{N_y}{R} \\ +p_0 + N_x w_{xx} + 2N_{xy} w_{xy} + N_y w_{yy} \\ -k_1 w + k_2(w_{xx} + w_{yy}) = 0 \end{matrix} \tag{14}$$

$$M_{x,x} + M_{xy,y} - Q_x + 3cR_x - c\left(P_{x,x} + P_{xy,y}\right) = 0 \tag{15}$$

$$M_{y,y} + M_{xy,x} - Q_y + 3cR_y - c\left(P_{y,y} + P_{xy,x}\right) = 0 \tag{16}$$

Here, the symbol p_0 represents the uniform external pressure. Additionally, K_1 and K_2 are the Kerr elastic foundation parameters, as described by Ebrahimi *et al*. (2024d).

The stress function $F(x, y)$ is introduced as (Ebrahimi *et al*. 2025c, 2024d):

$$F_{,yy} = N_x,\ F_{,xx} = N_y,\ F_{,xy} = -N_{xy} \tag{17}$$

Consequently, the strain components can be expressed in terms of ς and *w* as follows:

$$\begin{matrix} \epsilon_x^0 = \frac{A_{22}}{\Delta} F_{,yy} - \frac{A_{12}}{\Delta} F_{,xx} - \frac{A_{13}A_{22} - A_{14}A_{12}}{\Delta} k_x^1 \\ - \frac{A_{14}A_{22} - A_{24}A_{12}}{\Delta} k_y^1 - \frac{A_{15}A_{22} - A_{16}A_{12}}{\Delta} k_x^3 \\ - \frac{A_{16}A_{22} - A_{26}A_{12}}{\Delta} k_y^3 \\ \epsilon_y^0 = \frac{A_{11}}{\Delta} F_{,xx} - \frac{A_{12}}{\Delta} F_{,yy} - \frac{A_{11}A_{14} - A_{13}A_{12}}{\Delta} k_x^1 \\ - \frac{A_{11}A_{24} - A_{14}A_{12}}{\Delta} k_y^1 - \frac{A_{11}A_{16} - A_{15}A_{12}}{\Delta} k_x^3 \\ - \frac{A_{11}A_{26} - A_{16}A_{12}}{\Delta} k_y^3 \\ \gamma_{xy}^0 = -\frac{1}{A_{31}} F_{,xy} - \frac{A_{32}}{A_{31}} k_{xy}^1 - \frac{A_{33}}{A_{31}} k_{xy}^3 \end{matrix} \tag{18}$$

In which $\Delta = A_{11}A_{22} - A_{12}^2$

From Eq. (7), the deformation compatibility equation is established as:

$$\begin{matrix} \varepsilon_{x,yy}^0 + \varepsilon_{y,xx}^0 - \gamma_{xy,xy}^0 + \frac{1}{R} w_{,xx} + \frac{1}{a} w_{,yy} \\ - w_{,xy}^2 + w_{,xx} w_{,yy} = 0 \end{matrix} \tag{19}$$

Inserting Eq. (18) into Eq. (12) and utilizing the obtained expressions in Eqs. (13)-(16), the equilibrium equations can be derived as:

$$\begin{matrix} H_{11}(\phi_x) + H_{12}\left(\phi_y\right) + H_{13}(w) + H_{14}(F) \\ +P(w, F) + p_0 = 0 \end{matrix} \tag{20}$$

$$H_{21}(\phi_x) + H_{22}(\phi_y) + H_{23}(w) + L_{24}(F) = 0 \tag{21}$$

$$H_{31}(\phi_x) + H_{32}(\phi_y) + H_{33}(w) + L_{34}(F) = 0 \tag{22}$$

where

$$\begin{matrix} H_{11}(\varphi_x) = D_{11}\varphi_{x,x} + D_{12}\varphi_{x,xxx} + D_{13}\varphi_{y,xyy}, H_{12}\left(\varphi_y\right) \\ = D_{21}\varphi_{y,y} + D_{22}\varphi_{y,xxy} + D_{23}\varphi_{y,yyy} \\ H_{13}(w) = D_{31}w_{,xx} + D_{32}w_{,yy} + D_{33}w_{,xxxx} \\ +D_{34}w_{,yyyy} + D_{35}w_{,xxyy} - k_1 w + k_2\left(w_{,xx} + w_{,yy}\right) \\ H_{14}(F) = D_{11}^* F_{,xxxx} + D_{12}^* F_{,xxyy} + D_{13}^* F_{,yyyy} \\ + \frac{F_{,xx}}{R} + \frac{F_{,yy}}{a}, \\ H_{22}\left(\varphi_y\right) = D_{51}\varphi_{y,xy} \\ P(w, F) = F_{,yy}w_{,xx} - 2F_{,xy}w_{,xy} + F_{,yy}w_{,yy}, \\ H_{21}(\varphi_x) = D_{41}\varphi_x + D_{42}\varphi_{x,xx} + D_{43}\varphi_{x,xy} \\ H_{23}(w) = D_{61}w_{,x} + D_{62}w_{,xxx} + D_{63}w_{,xyy}, \\ H_{24}(F) = D_{21}^* F_{,xyy} + D_{22}^* F_{,xxx} \\ H_{31}(\varphi_x) = D_{71}\varphi_{x,xy}, \\ H_{32}\left(\varphi_y\right) = D_{81}\varphi_{y,yy} + D_{82}\varphi_{y,xx} + D_{83}\varphi_y \\ H_{33}(w) = D_{91}w_{,y} + D_{92}w_{,xxy} + D_{93}w_{,yyy}, \\ H_{34}(F) = D_{31}^* F_{,yyy} + D_{32}^* F_{,yxx} \end{matrix} \tag{23}$$

where the expressions of D_{ij} and D_{ij}^* are presented in Ebrahimi *et al*. (2024d) and Ebrahimi *et al*. (2025c). By inserting Eq. (18) into Eq. (19), we obtain the compatibility equation as:

$$\begin{matrix} I_1 F_{,yyyy} + I_2 F_{,xxxx} + I_3 F_{,xxyy} + I_4 F_{,yyy} + I_5 \phi_{x,xyy} \\ +I_6 \varphi_{x,xxx} + I_7 \varphi_{y,xxy} + I_8 w_{,xxxx} + I_9 w_{,yyyy} \\ +I_{10} w_{,xxyy} = w_{,xy}^2 - w_{,xx} w_{,yy} - \frac{w_{,xx}}{R} - \frac{w_{,yy}}{a} \end{matrix} \tag{24}$$

where the coefficients $I_j (j = 1, \ldots, 10)$ are provided in Ebrahimi *et al*. (2025c). Eqs. (20)-(22) and (24) represent the governing equations to investigate the thermo-mechanical stability behavior of the sandwich shells.

4. Solution procedure

Consider simply supported sandwich TSSs with freely movable edges, subjected to an external uniform pressure p_0 and thermal loading at boundary edges $x = 0$ and $x = L$. The boundary conditions are

$$w = 0, M_x = 0, N_x = 0, N_{xy} = 0, \phi_y = 0 \tag{25}$$

The solution of the deflection function satisfying the above boundary conditions in the average sense is assumed to be as follows (Ebrahimi *et al*. 2025c, 2024d):

$$w = W_0 + W_1 sin\frac{m\pi x}{L} sin\frac{ny}{R} + W_2 sin^2\frac{m\pi x}{L} \tag{26}$$

where W_0, W_1, and W_2 are the amplitudes of deflection. Furthermore, *m* and *n* represent the number of half-waves along the *x*- and *y*-directions. It is noted that while this study adopts simply supported boundaries, the approach may be extended to other boundary conditions by modifying the assumed displacement functions to satisfy the corresponding constraints.

Inserting Eq. (26) into the compatibility Eq. (24) and

solving the obtained equations for the unknown $F(x,y)$ yields:

$$\begin{aligned} F &= F_1\cos\left(\frac{2m\pi x}{L}\right)+F_2\cos\left(\frac{2ny}{R}\right)\\ &+F_3\sin\left(\frac{3m\pi x}{L}\right)\sin\left(\frac{ny}{R}\right)\\ &+F_4 sin(\frac{3m\pi x}{L})sin(\frac{ny}{R})-\frac{1}{2}\sigma_{0y}hx^2 \end{aligned} \tag{27}$$

where σ_{0y} denotes the negative average circumferential stress.

The stress function must satisfy Eqs. (21) and (22), which is achieved if ϕ_x and ϕ_y are defined as:

$$\begin{aligned} \phi_x(x,y) &= C_1\cos\left(\frac{m\pi x}{L}\right)\sin\left(\frac{ny}{R}\right)\\ &+C_2\sin\left(\frac{2m\pi x}{L}\right)+C_3\cos\left(\frac{3m\pi x}{L}\right)\sin\left(\frac{ny}{R}\right) \end{aligned} \tag{28a}$$

$$\begin{aligned} \phi_y(x,y) &= C_4\cos\left(\frac{ny}{R}\right)\sin\left(\frac{m\pi x}{L}\right)\\ &+C_5\cos\left(\frac{ny}{R}\right)\sin\left(\frac{3m\pi x}{L}\right)+C_6\sin\left(\frac{2ny}{R}\right) \end{aligned} \tag{28b}$$

Accordingly, by substituting Eqs. (27)-(28) into Eqs. (21)-(22) and solving the obtained expressions, the parameters $C_i(i=1,6)$ and $F_i(i=1,4)$ are determined as follows:

$$\begin{aligned} &F_1=-a_{15}W_2+a_{16}W_1^2,\ F_2=a_{12}W_1^2,\\ &F_3=-\frac{d_{26}W_1+(d_{15}d_{18}d_{22}-d_{15}d_{16}d_{20})W_1W_2}{d_{24}},\\ &F_4=b_{23}W_1W_2,\\ &C_1=-\frac{d_{25}W_1+(d_{15}d_{17}d_{20}+d_{15}d_{18}d_{21})W_1W_2}{d_{24}},\\ &C_2=a_{13}W_2-a_{14}W_1^2,\ C_3=b_{21}W_1W_2,\\ &C_4=-\frac{d_{27}W_1+(d_{15}d_{16}d_{21}+d_{15}d_{17}d_{22})W_1W_2}{d_{24}},\\ &C_5=b_{22}W_1W_2,\ C_6=a_{11}W_1^2 \end{aligned} \tag{29}$$

where the coefficients a_{ij}, b_{ij}, and d_{ij} are presented in Ebrahimi *et al*. (2025c) and Ebrahimi *et al*. (2024d).

Subsequently, substituting Eqs. (26)-(28) into Eqs. (20)-(22) and applying the Galerkin method yields:

$$q-K_1\left(W_0+\frac{W_2}{2}\right)-\frac{h}{R}\sigma_{0y}=0 \tag{30}$$

$$l_{11}+l_{12}W_1^2+l_{13}W_2+l_{14}W_2^2+hL^2n^2\sigma_{0y}=0 \tag{31}$$

$$K_1W_0+l_{16}W_1^2+l_{17}W_2+l_{18}W_1^2W_2+\frac{h}{R}\sigma_{0y}=P_0 \tag{32}$$

in which l_{ij} are defined as presented in Ebrahimi *et al*. (2024c). Furthermore, since the shells are circumferentially closed, the following condition must be satisfied:

$$\begin{aligned} &\int_0^{2\pi R}\int_0^L v_{,y}dxdy\\ &=\int_0^{2\pi R}\int_0^L\left(\varepsilon_y^0+\frac{w}{R}-\frac{1}{2}w_{,y}^2\right)dxdy=0 \end{aligned} \tag{33}$$

Using Eq. (18), Eq. (26), Eq. (27), and Eq. (28), this integral leads to

$$\begin{aligned} &\frac{(2W_0+W_2)}{R}-\left(\frac{n}{2R}\right)^2W_1^2-2hI_2\sigma_{0y}-\frac{2A_{12}\psi_1}{\Delta}\\ &+2I_2\psi_2=0 \end{aligned} \tag{34}$$

Substituting σ_{0y} from Eq. (30) into Eqs. (31)-(32), together with the application of the shell's circumferential closure condition, Eqs. (31)-(32) can be rewritten in the form:

$$W_0=S_{17}W_1^2-W_2/2+S_{18}P_0+S_{31}\psi_1-S_{32}\psi_2 \tag{35}$$

$$S_{11}+S_{12}W_0-S_{13}W_1^2+l_{14}W_2-S_{15}W_2^2-S_{16}p_0=0 \tag{36}$$

$$W_1^2=\frac{S_{22}W_2}{S_{21}-S_{23}W_2} \tag{37}$$

where the expressions of S_{ij} are presented in Ebrahimi *et al*. (2025c, 2024d).

$$\begin{aligned} P_0 &= \left\{\frac{S_{11}S_{22}-S_{31}S_{12}S_{22}\psi_1}{S_{22}-S_{23}W_2}+S_{12}S_{32}\psi_2\right.\\ &-S_{13}S_{21}-S_{12}S_{17}S_{21}+S_{14}S_{22}\\ &+\frac{+S_{12}S_{18}S_{22}-S_{11}S_{23}+S_{31}S_{12}S_{23}\psi_1}{S_{22}-S_{23}W_2}W_2\\ &+\frac{-S_{15}S_{22}-S_{14}S_{23}-S_{12}S_{18}S_{23}}{S_{22}-S_{23}W_2}W_2^2\\ &\left.+\frac{S_{15}S_{23}}{S_{22}-S_{23}W_2}W_2^3\right\}\times\left(\frac{1}{(S_{12}S_{19}-S_{16})}\right) \end{aligned} \tag{38}$$

By setting $W_2=0$ in Eq. (38), the upper buckling load of the sandwich shells can be obtained as

$$p_0^{\text{upper}}=\frac{S_{11}-S_{31}S_{12}\psi_1+S_{32}S_{12}\psi_2}{S_{12}S_{19}-S_{16}} \tag{39}$$

The critical buckling load is determined by minimizing p_0^{upper} from Eq. (39) with respect to *m* and *n*.

Utilizing Eqs. (35)-(37), the maximum deflection-nonlinear amplitude can be expressed as:

$$\begin{aligned} W_{\max} &= S_{17}W_1^2+\frac{W_2}{2}+S_{18}P_0+S_{31}\psi_1-S_{32}\psi_2\\ &+\left(\frac{S_{22}W_2}{S_{21}-S_{23}W_2}\right)^{1/2} \end{aligned} \tag{40}$$

Combining Eq. (38) and Eq. (40), the postbuckling curve P_0-W_{max}/h for sandwich composite TSSs can be obtained.

5. Different types of thermal loading

To comprehensively assess the effect of temperature variation across the thickness, different types of temperature distributions are considered, as described below:

Table 1 The critical buckling load $\bar{p}_{cr}$(kPa) of CNTRC cylindrical shells under external radial pressure ($\bar{V}_{CNT}$ = 0.17, *R/h* = 30, *h* = 2 mm)

	Shen *et al*. (2011b)		Present	
$T(K)$	300	500	300	500
$\bar{Z}=100$	776.63 (1,5)*	600.64 (1,5)	775.694 (1,5)	600.8 (1,5)
$\bar{Z}=300$	433.04(1,4)	325.10(1,4)	432.962(1,4)	324.621
$\bar{Z}=500$	343.81(1,4)	255.59(1,4)	343.748(1,4)	255.332(1,4)

*Numbers in parentheses denote the buckling modes (*m*, *n*)

Table 2 The critical buckling load p_0^{cr} (MPa) for CNTRC TSSs under external radial pressure (T = 300 K, *R/h* = 80, *h* = 1 mm, $h_2 = 2\ mm$, $K_1 = 10^7$, $K_2 = 10^5$)

Shell type	V_{CNT}	Van Tien *et al*. (2022)		Present (TSDT)	
		UD	FG-X	UD	FG-X
Convex	0.12	1.008 (1,5)	1.080 (1,5)	0.996405 (1,5)	1.0641 (1,5)
	0.17	1.219 (1,5)	1.325 (1,5)	1.1970 (1,5)	1.2957 (1,5)
Concave	0.12	0.825 (1,4)	0.871 (1,4)	0.820598 (1,4)	0.864437 (1,4)
	0.17	0.926 (1,4)	0.993 (1,4)	0.917225 (1,4)	0.980805 (1,4)

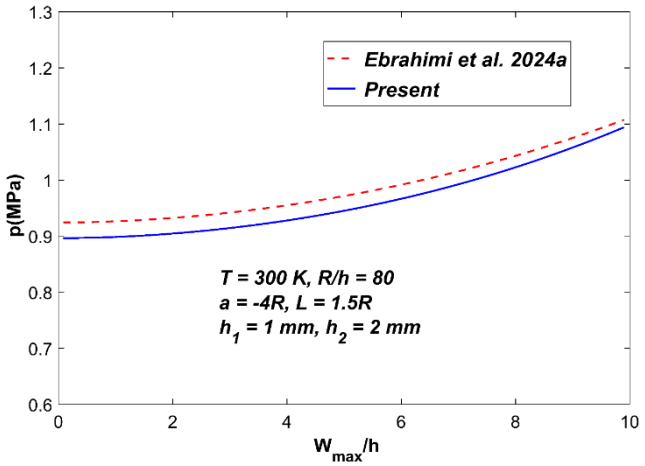

Fig. 3 Postbuckling curves for sandwich TSSs with bio-inspired and re-entrant honeycomb cores

5.1 Uniform temperature rise (UTR)

In this case, the initial temperature of the sandwich TSSs is assumed to be T_i, at which the shell is free from thermal strain. This temperature then increases to T_f. The temperature change is expressed as (Eslami *et al*. 2018, Hieu and Van Tung 2020c):

$$\Delta T = T_f - T_i \tag{41}$$

5.2 Linear temperature rise (LTR)

For a linear variation of temperature across the shell thickness, the temperature distribution is described as (Ebrahimi and Salari 2016, Eslami *et al*. 2018):

$$T = T_i + \Delta T\left(\frac{z}{h}+\frac{1}{2}\right) \tag{42}$$

Here, $\Delta T = T_o - T_i$, where T_o and T_i are the temperatures at the outer and inner surfaces, respectively.

5.3 Nonlinear temperature rise (NTR)

For a nonlinear temperature rise, where the temperature varies sinusoidally across the thickness, the temperature field is defined as (Ebrahimi and Barati 2016):

$$T = T_i + \Delta T\left(1 - \mathrm{Cos}\frac{\pi}{2}\left(\frac{z}{h}+\frac{1}{2}\right)\right) \tag{43}$$

6. Numerical results and discussion

6.1 Validation studies

Comparative analyses are conducted on three distinct shell geometries and material types to validate the proposed approach and confirm the method's accuracy.

Example 1. The first validation involves comparing the critical buckling loads of a CNTRC cylindrical shell (a→∞) under external pressure. The results are compared with those reported by Shen (2011b), which was conducted in the framework HSDT for different values of $\bar{Z} = L^2/Rh$ and different thermal environments. As shown in Table 1, the results align well with Shen's findings, validating the correctness and reliability of the proposed solution technique.

Example 2: The second validation involves a comparative analysis with the findings of Van Tien *et al*. (2022) for FG-CNTRC TSSs featuring a PMMA core, CNT-reinforced coatings, and an elastic foundation subjected to external pressure. The critical buckling loads in Table 2 align closely with the findings of Van Tien *et al*. (2022), demonstrating the precision and robustness of the proposed method.

Example 3: Further validation is carried out by comparing the results with the findings of Ebrahimi *et al*. (2024a) for CNTRC TSSs incorporating a re-entrant auxetic core and CNT-reinforced coatings under radial pressure. As shown in Fig. 3, the postbuckling curves derived from this study exhibit strong agreement with those reported by Ebrahimi *et al*. (2024a).

The input parameters for this comparison are $\bar{V}_{CNT} = 0.17$, uniform distribution (UD) along the *y*-direction for CNT reinforcement, $E_{matrix} = 2.5 \times 10^9$, $\nu_{matrix} = 0.34$, $K_1 = 10^7 N/m^3$, and $K_2 = 10^5 N/m$. The strong agreement further supports the reliability of the proposed approach.

6.2 Parametric analysis

The auxetic core layer of the sandwich TSSs uses aluminum alloy with temperature-dependent mechanical properties, where Young's modulus (E), thermal expansion coefficient (α), and Poisson ratio (ν_f) are defined by Li *et al*. (2019):

Table 3 The thermomechanical buckling loads p_0^{cr} (in MPa) of sandwich shells under UTR thermal loading ($\rho^*/\rho^s = 0.3,\ L = 1.5R, h = 1\ mm,\ h_2 = 2\ mm,\ K_l = K_u = 10^7,\ K_s = 10^5$

Shell type	ΔT(K)	R/h	Butterfly-shaped auxetic core	Re-entrant auxetic core	Difference (%)
Convex shell ($a = 4R$)	50	100	0.633791	0.602685	5.16*
		60	1.56447	1.46213	7.00
		20	16.0249	14.0453	14.09
	100	100	0.622952	0.59256	5.13
		60	1.53037	1.43007	7.01
		20	15.7122	13.7306	14.43
	200	100	0.602139	0.57313	5.06
		60	1.46474	1.3683	7.05
		20	15.1271	13.1272	15.23
Concave shell ($a = -4R$)	50	100	0.450404	0.447982	0.54
		60	0.993336	0.965342	2.90
		20	12.0251	10.849	10.84
	100	100	0.449022	0.446597	0.54
		60	0.982256	0.954777	2.88
		20	11.6335	10.4783	11.02
	200	100	0.446843	0.444393	0.55
		60	0.961592	0.935068	2.84
		20	10.8675	9.75062	11.45

*Difference = $100\%[P_{cr}^{butterfly-shaped} - P_{cr}^{re-entrant}]/P_{cr}^{re-entrant}$

Table 4 The thermomechanical buckling loads p_0^{cr} (in MPa) of sandwich shells with bio-inspired and honeycomb cores under LTR thermal loading ($\rho^*/\rho^s = 0.3,\ L = 1.5R, h = 1\ mm,\ h_2 = 2\ mm,\ K_l = K_u = 10^7,\ K_s = 10^5$)

Shell type	T_o	R/h	Butterfly-shaped auxetic core	Re-entrant auxetic core	Difference (%)
Convex shell ($a = 4R$)	350	100	0.640743	0.60858(1,5)	5.28
		60	1.58627	1.48095(1,4)	7.11
		20	16.2272	14.2544(1,3)	13.84
	400	100	0.636628	0.60414(1,5)	5.38
		60	1.57331	1.46712 (1,4)	7.24
		20	16.1066	14.1421 (1,3)	13.89
	500	100	0.628784	0.595652 (1,5)	5.56
		60	1.54859	1.44063 (1,4)	7.49
		20	15.8841	13.9321(1,3)	14.01
Concave shell ($a = -4R$)	350	100	0.451251(1,4)	0.448835 (1,4)	0.54
		60	1.00051 (1,3)	0.971744 (1,3)	2.96
		20	12.2775 (1,2)	11.071 (1,2)	10.90
	400	100	0.450562 (1,4)	0.448154 (1,4)	0.54
		60	0.99622 (1,3)	0.967226 (1,3)	3.00
		20	12.1344 (1,2)	10.9192 (1,2)	11.13
	500	100	0.449432 (1,4)	0.44703 (1,4)	0.54
		60	0.988338 (1,3)	0.958867 (1,3)	3.07
		20	11.8575 (1,2)	10.6238 (1,2)	11.61

$$E = 69000(1 - 0.00053\Delta T)\ \text{GPa}$$
$$\alpha = 23.0(1 + 0.00072)\Delta T \times 10^{-6}/\,^{\circ}\text{C} \quad (44)$$
$$v_f = 0.33$$

The CNT-reinforced face sheets in this study are modeled with a Poly (methyl methacrylate) (PMMA) matrix. The temperature-dependent material properties of the CNT, the matrix, and the efficiency parameters of the CNT are

Table 5 The thermomechanical buckling loads p_0^{cr} (in MPa) of sandwich shells with bio-inspired and re-entrant honeycomb cores under NTR thermal loading ($\rho^*/\rho^s = 0.3$, $L = 1.5R$, h = 1 mm, $h_2 = 2\,mm$, $K_l = K_u = 10^7$, $K_s = 10^5$)

Shell type	T_o	*R/h*	Butterfly auxetic core	Re-entrant auxetic core	Difference
Convex shell ($a = 4R$)	350	100	0.639704 (1,5)	0.60767 (1,5)	5.27
		60	1.58308 (1,4)	1.47811 (1,4)	7.10
		20	16.1996 (1,3)	14.2253 (1,3)	13.88
	400	100	0.634584 (1,5)	0.602353 (1,5)	5.35
		60	1.56703 (1,4)	1.46155 (1,4)	7.22
		20	16.053 (1,3)	14.0853 (1,3)	13.97
	500	100	0.624794 (1,5)	0.592179 (1,5)	5.51
		60	1.53632 (1,4)	1.42979 (1,4)	7.45
		20	15.7816 (1,3)	13.8227 (1,3)	14.17
Concave shell ($a = -4R$)	350	100	0.451139 (1,4)	0.448721 (1,4)	0.54
		60	0.999534 (1,3)	0.970859 (1,3)	2.95
		20	12.2431 (1,2)	11.04 (1,2)	10.90
	400	100	0.450359 (1,4)	0.447946 (1,4)	0.54
		60	0.994331 (1,3)	0.965512 (1,3)	2.98
		20	12.0663 (1,2)	10.8579 (1,2)	11.13
	500	100	0.449087 (1,4)	0.446677 (1,4)	0.54
		60	0.984729 (1,3)	0.955609 (1,3)	3.05
		20	11.7235 (1,2)	10.5033 (1,2)	11.62

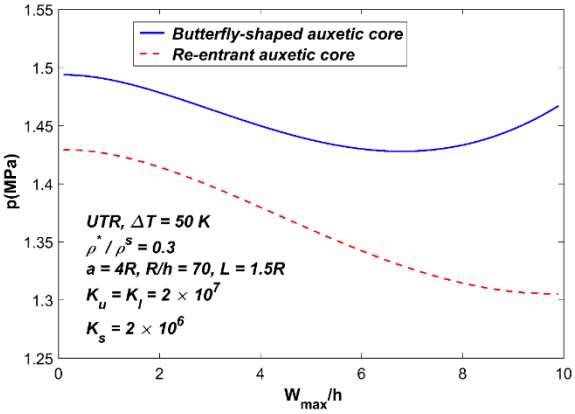

Fig. 4 Postbuckling curves of convex TSSs with bio-inspired and re-entrant honeycomb cores

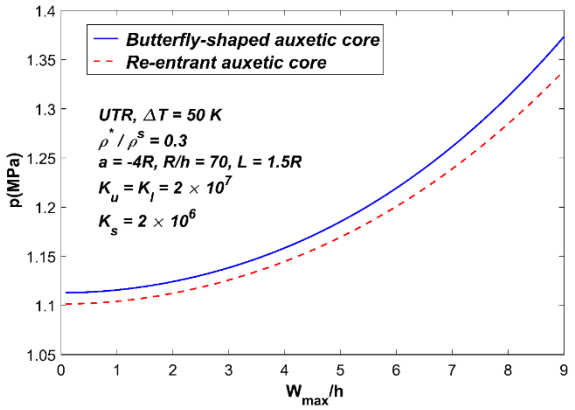

Fig. 5 Postbuckling curves of concave TSSs with bio-inspired and honeycomb cores

based on the results of Shen (2011a, b) and Shen and Xiang (2013). The CNTs are aligned circumferentially in the shell's face sheet with a fixed volume fraction ($\bar{V}_{CNT} = 0.17$). Furthermore, each face sheet is assumed to have a uniform thickness of 1 mm.

In this study, the material properties of the CNTRC face sheets are adopted from Shen (2011b), assuming a constant room temperature of 300 K. Additionally, the parameters of the Kerr foundation are selected based on established models in the literature, particularly those proposed by Ebrahimi *et al*. (2024d, 2025c).

6.3 Effect of auxetic core types under various thermal loading conditions

This section compares the thermomechanical stability of sandwich shells with auxetic cores, including re-entrant honeycomb and butterfly-shaped structures, under varying R/h ratios. The results, presented in Tables 3-5, are evaluated under different thermal conditions, assuming an equal relative density ($\rho^*/\rho^s = 0.3$). The initial temperature (T_i) is set to 300 K for UTR conditions, with uniform increments (ΔT) of 50, 100, and 200 K. Under NTR and LTR conditions, the shell's inner surface is maintained at $T_i = 300\text{K}$, while the outer surface temperature (T_o) increases to 350, 400, and 500 K.

The findings indicate the superior performance of the butterfly-shaped structure compared to the conventional re-entrant type for both Gaussian curvatures for every *R/h* value and thermal condition. For instance, under LTR thermal loading, at $R/h = 100$ and $T_o = 350\,\text{K}$, the

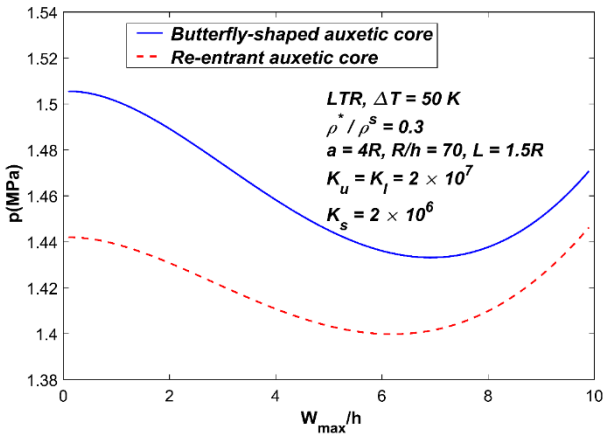

Fig. 6 Postbuckling curves of convex TSSs with bio-inspired and re-entrant honeycomb cores under LTR

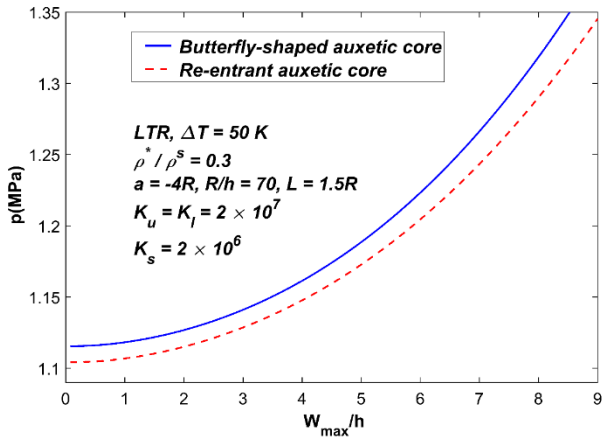

Fig. 7 Postbuckling curves of concave TSSs with bio-inspired and re-entrant honeycomb cores under LTR

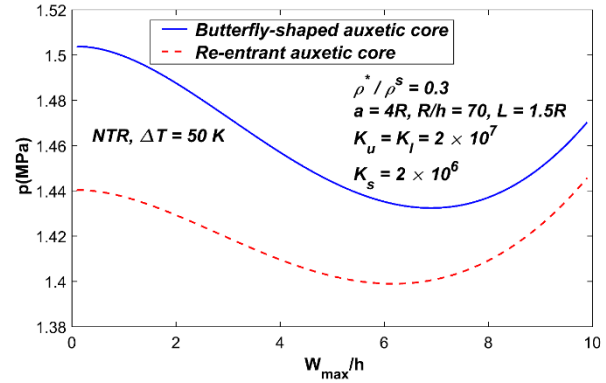

Fig. 8 Postbuckling curves of convex TSSs with bio-inspired and re-entrant honeycomb cores under NTR

sandwich shells with the bio-inspired type demonstrate a 5.28% enhancement in thermomechanical critical buckling load compared to those with the re-entrant auxetic core. This difference becomes more pronounced for thicker shells and higher thermal rises. Specifically, at $R/h = 20$ and the same temperature rise, the enhancement reaches 14.09%, further increasing to 15.23% at $T_o = 500$ K. A similar trend is observed for concave TSSs, where under identical geometric and material conditions, the thermomechanical

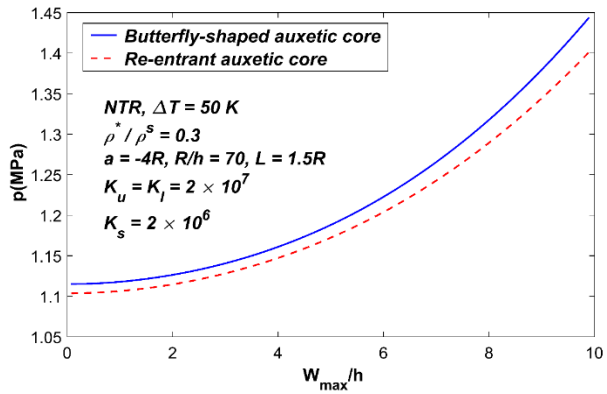

Fig. 9 Postbuckling curves of concave TSSs with bio-inspired and re-entrant honeycomb cores under NTR

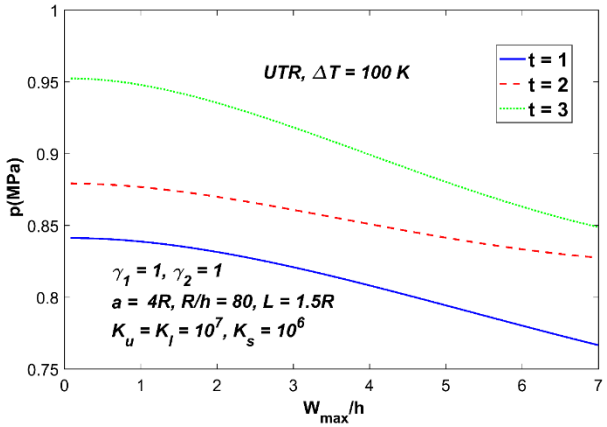

Fig. 10 Effect of cell rib thickness on the postbuckling curves of convex shells

buckling loads show a 0.54% improvement at $R/h = 100$, rising to 10.90% at $R/h = 20$ for $T_o = 350$ K and further increasing to 15.23% at $T_o = 500$ K.

The comparative analysis of the postbuckling response of sandwich shells with re-entrant honeycomb and butterfly-shaped structures is presented in Figs. 4-9 for a fixed relative density. This analysis encompasses both Gaussian curvatures and considers all thermal conditions (UTR, LTR, and NTR). The results demonstrate that, in the entire range of $W_{\max}/h$, the postbuckling curves of the butter-shaped auxetic core consistently exhibit higher values and enhanced stability over the honeycomb type, highlighting its improved performance. Moreover, the snap-through phenomenon, commonly observed in convex shells, is notably absent in concave shells.

6.4 parametric study of the butterfly-shaped auxetic unit cell

Alterations in the geometrical parameters of the bio-inspired unit cell can markedly affect the stability performance of sandwich shells. The following analysis presents a detailed assessment of these parameters. The parameters studied include the rib length ratio $\gamma_1 = l_3/l_1$, the angle ratio $\gamma_2 = \theta/\theta_1$, and the rib thickness t (see Fig. 2). The analysis considers variations under UTR conditions, with a constant rib length (l_1 = 0.008 mm) and angle (θ = 60°).

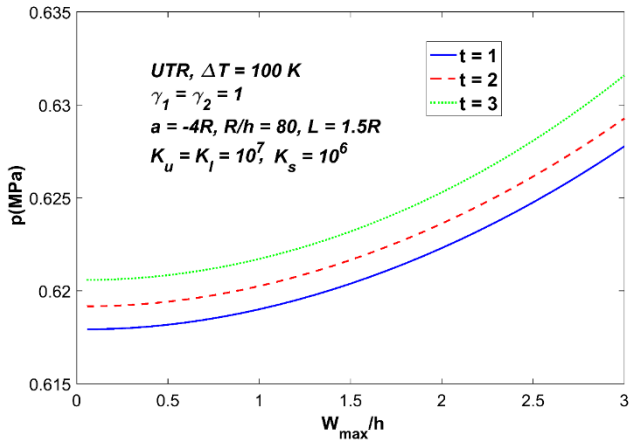

Fig. 11 Effect of cell rib thickness on the postbuckling curves of concave shells

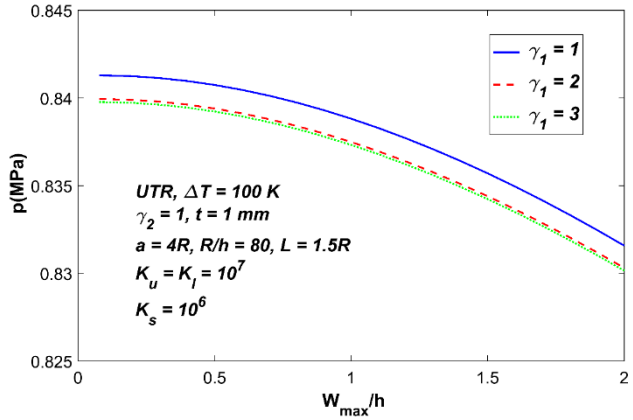

Fig. 12 Effect of $\boldsymbol{\gamma_1}$ on the postbuckling curves of convex shells

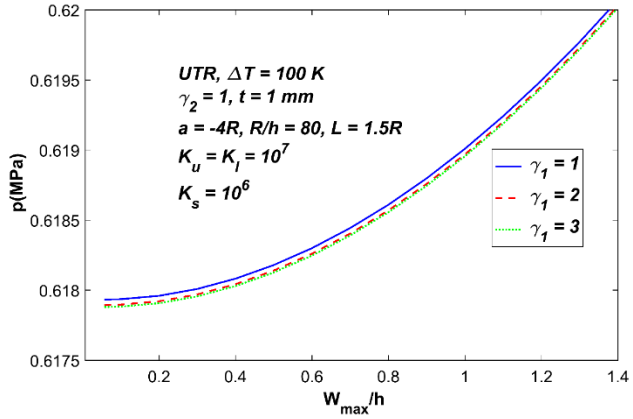

Fig. 13 Effect of $\boldsymbol{\gamma_1}$ on the postbuckling curves of concave shells

Figs. 10 and 11 demonstrate the influence of t on the postbuckling characteristics of the shells under thermo-mechanical loading. Increasing t enhances both shell types' buckling and postbuckling resistance. For example, with $\gamma_1 = \gamma_2 = 1$ under UTR thermal conditions, the critical buckling load of convex sandwich shells increases from 0.8413 MPa at 1 mm to 0.8793 MPa at 3 mm and 0.9524 MPa at 5 mm, an overall improvement of 13.21%. For the

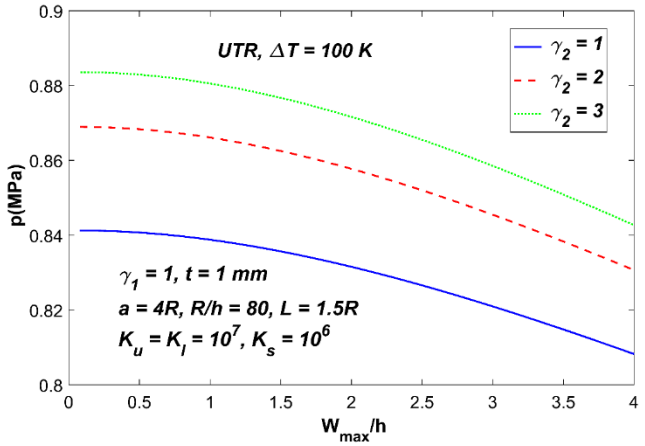

Fig. 14 Effect of $\boldsymbol{\gamma_2}$ on the postbuckling curves of convex shells

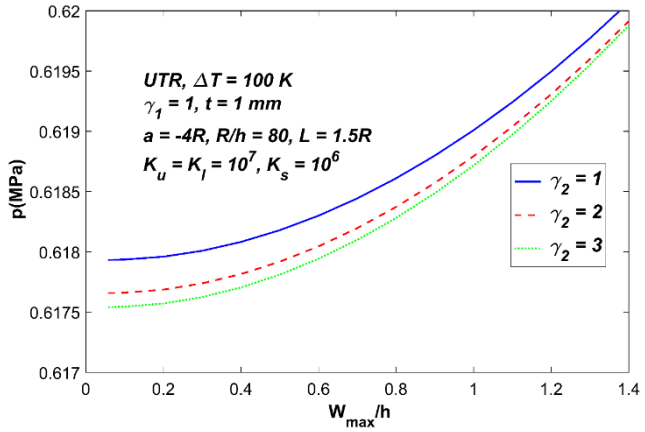

Fig. 15 Effect of $\boldsymbol{\gamma_2}$ on the postbuckling curves of concave shells

concave shell, the increase is marginal, with values rising from 0.6179 MPa to 0.6206 MPa, reflecting a 0.44% enhancement.

Figs. 12 and 13 illustrate the effects of the rib length ratio γ_1 on stability for t = 1 mm, $\gamma_2 = 1$, and UTR conditions. Increasing γ_1 reduces the critical buckling load and shifts postbuckling curves downward for both shell types. For convex shells, the critical buckling load decreases slightly from 0.8413 MPa at $\gamma_1 = 1$ to 0.8399 MPa and 0.8398 MPa at $\gamma_1 = 2$ and 3, respectively—a reduction of 0.18%. The reduction becomes more pronounced at higher t and γ_2, reaching 14.53% at t = 5 mm and $\gamma_2 = 3$. Concave shells show a similar trend, with reduced critical buckling loads and downward shifts in postbuckling curves (Fig. 13).

The impact of the angle ratio γ_2 varies between shell types (Figs. 14 and 15). For convex shells, increasing γ_2 raises critical buckling loads and shifts postbuckling curves upward. For instance, Fig. 14 shows that as γ_2 increases from 1 to 3, the critical buckling load rises from 0.8413 MPa to 0.8689 MPa and 0.8836 MPa, a 5.03% improvement, which is amplified at higher t. Conversely, for concave shells, increasing γ_2 reduces critical buckling loads and weakens postbuckling resistance (Fig. 15).

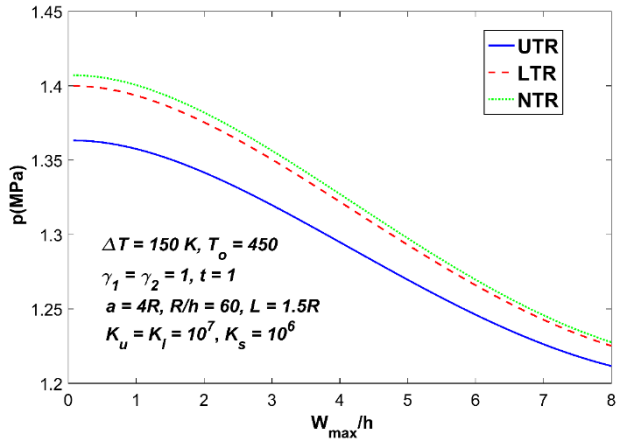

Fig. 16 Effect of different thermal loading conditions on the postbuckling responses of convex shells

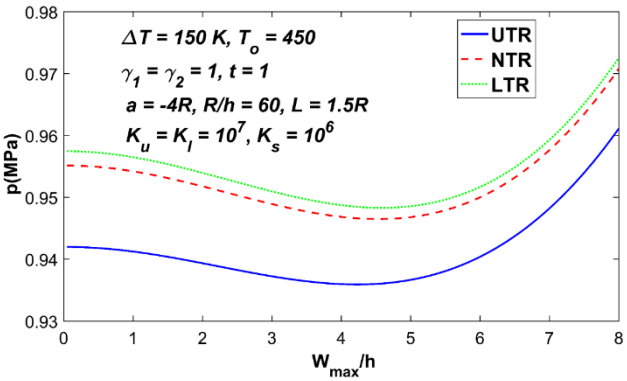

Fig. 17 Effect of different thermal loading conditions on the postbuckling responses of concave shells

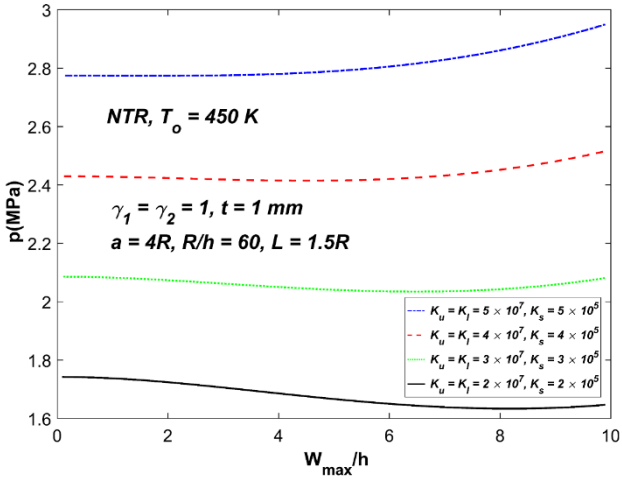

Fig. 18 Postbuckling curves of convex shells with varying foundation stiffnesses

6.5 Effects of different types of thermal loading

To investigate the effects of various thermal loading types on the stability of auxetic-core sandwich TSSs, critical thermal buckling loads from Tables 3-5 for UTR, LTR, and sinusoidal NTR temperature profiles under different thermal increments are compared. The analysis reveals that UTR has the most detrimental impact on

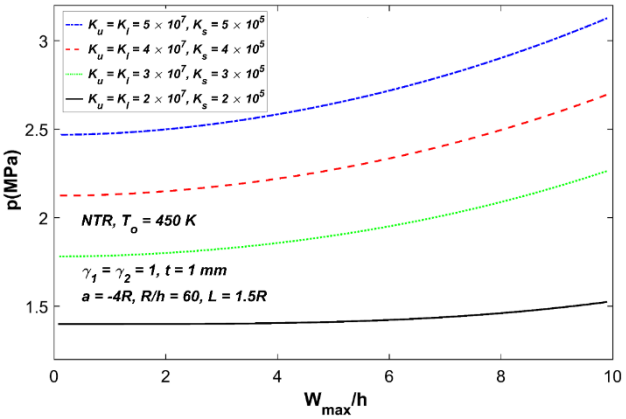

Fig. 19 Postbuckling curves of concave shells with varying foundation stiffnesses

reducing buckling loads, while LTR has the least effect for both convex and concave shell types. Figs. 16 and 17 also illustrate the postbuckling behavior under these thermal conditions, assuming an outer surface temperature of $T_o = 450$ K with auxetic geometric parameters $\gamma_1 = \gamma_2 = 1$ and $t = 1$ mm. For convex shells, the critical buckling loads under UTR, NTR, and LTR are reported as 1.3633, 1.4000, and 1.4071, respectively, showing reductions of 2.62% and 3.11% for UTR relative to NTR and LTR (Fig. 16). Similarly, for concave shells, the critical buckling loads are 0.9420, 0.9552, and 0.9575 for UTR, NTR, and LTR, respectively, with reductions of 1.62% and 1.38% for UTR relative to NTR and LTR (Fig. 17). Furthermore, the figures demonstrate that the load-carrying capacity exhibits the most significant drop under UTR, followed by NTR and LTR, for both convex and concave shells.

6.6 Influence of Kerr foundation

Figs. 18 and 19 illustrate how the Kerr foundation enhances the shells' postbuckling stability. Increasing the stiffness of the Kerr foundation significantly enhances the shells' stability, load-bearing capacity, and resistance to snap-through under thermomechanical loading. For instance, under NTR thermal conditions at $T_o = 450$ K, Fig. 18 demonstrates that higher stiffness parameters in the Kerr elastic foundation improve the postbuckling path. Notably, at $K_u = K_l = 5 \times 10^7$ and $K_s = 5 \times 10^5$, no snap-through phenomenon is observed. In concave sandwich shells, which are inherently less prone to snap-through behavior, the results further indicate that increasing the stiffness of the Kerr elastic foundation raises the postbuckling path, hence enhancing both load-carrying capacity and overall performance of the structure. These results emphasize the positive impact of a Kerr elastic foundation in mitigating the adverse effects of thermal loading by enhancing structural stiffness.

7. Conclusions

This paper presents an analytical approach to investigate the thermomechanical buckling and postbuckling behavior

of sandwich TSSs incorporating a bio-inspired NPR core with CNTRC face sheets surrounded by a Kerr elastic foundation. Three practical temperature conditions (UTR, LTR, and NTR) are examined, considering shell thickness variations. Formulations are established within the framework of TSDT, incorporating von Kármán-type nonlinearity and the Airy stress function. The Galerkin method is utilized to obtain the load-deflection expressions. The numerical findings reveal several important observations:

1. The auxetic core with a butterfly-shaped design offers better performance over the traditional re-entrant type under all thermal conditions and *R/h* ratios for both positive and negative Gaussian curvatures. Under LTR thermal loading at $T_o = 500\,\mathrm{K}$ and $R/h = 20$, a 15.23% improvement in critical buckling load is achieved compared to the re-entrant core. Enhanced stability and elevated postbuckling curves also highlight its superiority.

2. Thermal loading conditions significantly influence stability, with UTR causing the greatest reduction in critical buckling loads, while LTR results in the least reduction. Postbuckling analysis also reveals the most pronounced drop in load-carrying capacity under UTR.

3. An increase in the rib thickness parameter *t* leads to higher critical buckling loads and improved postbuckling strength of both convex and concave TSSs under thermo-mechanical loading. Convex shells, in particular, exhibit a 13.21% increase in critical buckling load under UTR conditions.

4. Increasing the geometric parameter γ_1 reduces the critical buckling load and lowers postbuckling paths for both types of TSSs. These reductions become more significant at higher *t* and γ_2, reaching up to 14.53% for *t* = 5 mm and $\gamma_2 = 3$.

5. The angle ratio γ_2 has distinct effects depending on shell type. For convex shells, increasing γ_2 improves critical buckling loads and raises postbuckling curves, with a 5.03% increase in buckling load (from 0.8413 MPa to 0.8836 MPa) as γ_2 increases from 1 to 3, especially at higher *t*. Conversely, for concave shells, higher γ_2 reduces critical buckling loads and weakens postbuckling strength.

6. The Kerr elastic foundation significantly enhances the postbuckling stability and load-bearing capacity of butterfly-shaped auxetic-core sandwich TSSs under thermomechanical loading. It mitigates thermal effects by improving postbuckling curves and preventing snap-through. For instance, under NTR conditions at $K_u = K_l = 5 \times 10^7$ and $K_s = 5 \times 10^5$, no snap-through is observed.

References

Ashby, M.F. and Gibson, L.J. (1997), "Cellular solids: structure and properties", *Press Syndicate Univ. Cambridge*, 175-231, Cambridge, U.K. https://doi.org/10.1017/CBO9781139878326

Chakraborty, S. and Dey, T. (2023), "Thermomechanical buckling and wrinkling characteristics of softcore sandwich panels with CNT reinforced composite face sheets", *Eur. J. Mech. A Solids*, **98**, 104894. https://doi.org/10.1016/j.euromechsol.2022.104894

Chen, Z., Wang, A., Qin, B., Wang, Q. and Zhong, R. (2020), "Investigation on free vibration and transient response of functionally graded graphene platelets reinforced cylindrical shell resting on elastic foundation", *Eur. Phys. J. Plus*, **135**(7), 582. https://doi.org/10.1140/epjp/s13360-020-00577-4

Duc, N.D., Kim, S.E., Quan, T.Q., Manh, D.T. and Cuong, N.H. (2020), "Nonlinear buckling of eccentrically stiffened nano-composite cylindrical panels in thermal environments", *Thin Wall. Struct.*, **146**, 106428. https://doi.org/10.1016/j.tws.2019.106428

Dung, D.V. and Vuong, P.M. (2017), "Analytical investigation on buckling and postbuckling of FGM toroidal shell segment surrounded by elastic foundation in thermal environment and under external pressure using TSDT", *Acta Mechanica*, **228**(10), 3511-3531. https://doi.org/10.1007/s00707-017-1888-2

Ebrahimi, F. (2024), *Mechanics of Auxetic Materials and Structures*, CRC Press.

Ebrahimi, F., Goudarzfallahi, M. and Ziazi, A.A. (2024a), "Static stability analysis of graphene origami-reinforced nanocomposite toroidal shells with various auxetic cores", *Adv. Nano Res.*, **17**(1), 1. https://doi.org/10.12989/anr.2024.17.1.001

Ebrahimi, F., Goudarzfallahi, M. and Ziazi, A.A. (2024b), "Buckling and post-buckling analysis of sandwich toroidal shell composites with graphene origami-enabled auxetic metamaterial core under combined mechanical loads", *Compos. Mech. Comput. Appl. Int. J.*, Forthcoming Articles. https://doi.org/10.1615/CompMechComputApplIntJ.2024054751

Ebrahimi, F., Goudarzfallahi, M. and Ziazi, A.A. (2024c), "Porosity effects on the buckling and post buckling of metamaterial sandwich toroidal shell segments", *Steel Compos. Struct.*, **53**(3), 313-326. https://doi.org/10.12989/scs.2024.53.3.313

Ebrahimi, F., Goudarzfallahi, M. and Ziazi, A.A. (2024d), "Nonlinear stability analysis of shear-deformable sandwich meta-composite shell with arc-type auxetic core.", *Adv. Nano Res.*, **17**(6), 547. https://doi.org/10.12989/anr.2024.17.6.547

Ebrahimi, F., Goudarzfallahi, M. and Alinia Ziazi, A. (2025a). "Buckling and postbuckling analysis of graphene origami–enabled auxetic metamaterial sandwich toroidal shell segments subjected to axial compression", *J. Eng. Mech.*, **151**(5), 04025012. https://doi.org/10.1061/JENMDT.EMENG-7954

Ebrahimi, F., Goudarzfallahi, M. and Ziazi, A.A. (2025b), "Enhancing nonlinear static stability behavior of axially compressed sandwich composite toroidal shells with a bio-inspired auxetic core", *Acta Mechanica*, 1-18.

Ebrahimi, F., Goudarzfallahi, M. and Ziazi, A.A. (2025c), "Comparative analysis of nonlinear buckling and postbuckling in shear-deformable sandwich composite toroidal shell segments with diverse auxetic cores and CNT-reinforced face sheets", *Arch. Civil Mech. Eng.*, **25**(3), 154.

Ebrahimi, F., Goudarzfallahi, M. and Ziazi, A.A. (2025d), "Assessing the effect of stiffeners on the stability of sandwich metacomposite toroidal shells under axial compression", *Adv. Aircr. Spacecr. Sci.*, **11**(4), 363-382.

Ebrahimi, F. and Dabbagh, A. (2023), "Porosity effects on static performance of carbon nanotube-reinforced meta-nanocomposite structures", *Micromachines*, **14**(7), 1402. https://doi.org/10.3390/mi14071402

Ebrahimi, F. and Dadashi, M. (2023), "Composite cylindrical shells with auxetic core on elastic foundation: A nonlinear dynamic analysis", *Structures*, **57**, 105170. https://doi.org/10.1016/j.istruc.2023.105170

Ebrahimi, F. and Ahari, M.F. (2024), "On the buckling of meta-graphene-origami-enabled magnetostrictive nanoplates under temperature gradient", *Acta*, 1-18. https://doi.org/10.1007/s00707-024-03861-x

Ebrahimi, F. and Dabbagh, A. (2020), *Mechanics of Nanocomposites: Homogenization and Analysis*, CRC Press.

Ebrahimi, F. and Barati, M.R. (2016), "Temperature distribution effects on buckling behavior of smart heterogeneous nanosize plates based on nonlocal four-variable refined plate theory", *Int.*

J. Smart Nano Mater., **7**(3), 119-143. https://doi.org/10.1080/19475411.2016.1223203

Ebrahimi, F. and Salari, E. (2016), "Effect of various thermal loadings on buckling and vibrational characteristics of nonlocal temperature-dependent functionally graded nanobeams", *Mech. Adv. Mater. Struct.*, **23**(12), 1379-1397. https://doi.org/10.1080/15376494.2015.1091524

Eslami, M.R., Eslami, J. and Jacobs, M. (2018), *Buckling and Postbuckling of Beams, Plates, and Shells*, Springer International Publishing, Switzerland.

Ezzati, H., Pashalou, S., Rastgoo, A. and Ebrahimi, F. (2024), "Vibration analysis of multilayer graphene origami-enabled metamaterial plates", *Acta Mechanica*, **235**, 7623-7640. https://doi.org/10.1007/s00707-024-04117-4

Fu, T., Wang, X., Hu, X. and Rabczuk, T. (2024), "Impact dynamic response of stiffened porous functionally graded materials sandwich doubly-curved shells with Arc-type auxetic core", *Int. J. Impact Eng.*, **191**, 105000. https://doi.org/10.1016/j.ijimpeng.2024.105000

Ghafouri, M., Ghassabi, M. and Talebitooti, R. (2023), "Applying a 3D re-entrant auxetic cellular core to a graphene nanoplatelet–reinforced doubly curved structure: A sound transmission loss study", *J. Eng. Mech.*, **149**(10), 04023077. https://doi.org/10.1061/JENMDT.EMENG-6978

Hieu, P.T. and Van Tung, H. (2021), "Thermal buckling and postbuckling of CNT-reinforced composite cylindrical shell surrounded by an elastic medium with tangentially restrained edges", *J. Thermoplast. Compos. Mater.*, **34**(7), 861-883. https://doi.org/10.1177/0892705719853611

Hieu, P.T. and Van Tung, H. (2020a), "Buckling of shear deformable FG-CNTRC cylindrical shells and toroidal shell segments under mechanical loads in thermal environments", *ZAMM J. Appl. Math. Mech.*, **100**(11), e201900243. https://doi.org/10.1177/0892705719853611

Hieu, P.T. and Van Tung, H. (2020b), "Thermal and thermomechanical buckling of shear deformable FG-CNTRC cylindrical shells and toroidal shell segments with tangentially restrained edges", *Arch. Appl. Mech.*, **90**(7), 1529-1546. https://doi.org/10.1007/s00419-020-01682-7

Hieu, P.T. and Van Tung, H. (2020c), "Thermomechanical postbuckling of pressure-loaded CNT-reinforced composite cylindrical shells under tangential edge constraints and various temperature conditions", *Polym. Compos.*, **41**(1), 244-257. https://doi.org/10.1002/pc.25365

Hoai Nam, V., Ngoc Ly, L., Thi Kieu My, D., Minh Duc, V. and Thi Phuong, N. (2024), "On the nonlinear buckling and postbuckling responses of sandwich FG-GRC toroidal shell segments with corrugated core under axial tension and compression in the thermal environment", *Polym. Compos.*, **45**(15), 13737-13752. https://doi.org/10.1002/pc.28732

Hutchinson, J.W. (1967), "Initial post-buckling behavior of toroidal shell segments", *Int. J. Solids Struct.*, **3**(1), 97-115. https://doi.org/10.1016/0020-7683(67)90046-7

Lakes, R. (1987), "Foam structures with a negative Poisson's ratio", *Science*, **235**(4792), 1038-1040.

Li, Y.S. and Liu, B.L. (2022), "Thermal buckling and free vibration of viscoelastic functionally graded sandwich shells with tunable auxetic honeycomb core", *Appl. Math. Modell.*, **108**, 685-700. https://doi.org/10.1016/j.apm.2022.04.019

Li, C., Shen, H.S. and Yang, J. (2022), "Low-velocity impact response of cylindrical sandwich shells with auxetic 3D double-V meta-lattice core and FG GRC facesheets", *Ocean Eng.*, **262**, 112299. https://doi.org/10.1016/j.oceaneng.2022.112299

Li, C., Shen, H.S. and Wang, H. (2019), "Nonlinear bending of sandwich beams with functionally graded negative Poisson's ratio honeycomb core", *Compos. Struct.*, **212**, 317-325. https://doi.org/10.1016/j.compstruct.2019.01.020

Nam, V.H., Duc, V.M., Doan, C.V., Thanh Xuan, N.T. and Phuong, N.T. (2022), "Nonlinear postbuckling behavior of auxetic-core toroidal shell segments with Graphene reinforced face sheets under axial loads", *Arch. Mech.*, **74**(2-3). http://doi.org/10.24423/aom.3957

Nguyen, T.P., Vu, M.D., Dang, T.D., Cao, V.D., Pham, T.H. and Vu, H.N. (2023), "An analytical approach of nonlinear buckling behavior of torsionally loaded auxetic core toroidal shell segments with graphene reinforced polymer coatings", *Adv. Compos. Mater.*, **32**(3), 400-418. https://doi.org/10.1080/09243046.2022.2110661

Nguyen, V.L., Tran, M.T., Limkatanyu, S., Mohammad-Sedighi, H. and Rungamornrat, J. (2022), "Reddy's third-order shear deformation shell theory for free vibration analysis of rotating stiffened advanced nanocomposite toroidal shell segments in thermal environments", *Acta Mechanica*, **233**(11), 4659-4684. https://doi.org/10.1007/s00707-022-03347-8

Nguyen, V.L., Limkatanyu, S., Bui, T.Q. and Rungamornrat, J. (2023a), "Free vibration analysis of rotating stiffened functionally graded graphene-platelet-reinforced composite toroidal shell segments with novel four-unknown refined theories", *Int. J. Mech. Mater. Des.*, **19**(2), 319-350. https://doi.org/10.1007/s10999-022-09626-5

Nguyen, V.L., Limkatanyu, S., Thai, H.T. and Rungamornrat, J. (2024), "Simple first-order shear deformation theory for free vibration of FGP-GPLRC spherical shell segments", *Mech. Adv. Mater. Struct.*, **31**(25), 6944-6961. https://doi.org/10.1080/15376494.2023.2240579

Phuong, N.T., Van Doan, C., Duc, V.M., Giang, N.T. and Nam, V. H. (2023), "Analytical solution for nonlinear buckling of convex and concave auxetic-core toroidal shell segments with graphene-reinforced face sheets subjected to radial loads", *Arch. Appl. Mech.*, **93**(2), 621-634. https://doi.org/10.1007/s00419-022-02288-x

Phuong, N.T., Nam, V.H., Trung, N.T., Duc, V.M., Van Loi, N., Thinh, N.D. and Tu, P.T. (2021), "Thermomechanical postbuckling of functionally graded graphene-reinforced composite laminated toroidal shell segments surrounded by Pasternak's elastic foundation", *J. Thermoplast. Compos. Mater.*, **34**(10), 1380-1407. https://doi.org/10.1177/0892705719870593

Qin, B., Wang, Q., Zhong, R., Zhao, X. and Shuai, C. (2020), "A three-dimensional solution for free vibration of FGP-GPLRC cylindrical shells resting on elastic foundations: A comparative and parametric study", *Int. J. Mech. Sci.*, **187**, 105896. https://doi.org/10.1016/j.ijmecsci.2020.105896

Reddy, J.N. and Liu, C.F. (1987), *A Higher-Order Theory for Geometrically Nonlinear Analysis of Composite Laminates*, No. VPI-E-86.21, NASA.

Reddy, J.N. (2003), *Mechanics of Laminated Composite Plates and Shells: Theory and Analysis*, CRC press.

Shen, H.S. (2011a), "Postbuckling of nanotube-reinforced composite cylindrical shells in thermal environments, Part I: Axially-loaded shells", *Compos. Struct.*, **93**(8), 2096-2108. https://doi.org/10.1016/j.compstruct.2011.02.011

Shen, H.S. (2011b), "Postbuckling of nanotube-reinforced composite cylindrical shells in thermal environments, Part II: Pressure-loaded shells", *Compos. Struct.*, **93**(10), 2496-2503. https://doi.org/10.1016/j.compstruct.2011.04.005

Shen, H.S. and Xiang, Y. (2013), "Postbuckling of nanotube-reinforced composite cylindrical shells under combined axial and radial mechanical loads in thermal environment", *Compos. Part B Eng.*, **52**, 311-322. https://doi.org/10.1016/j.compositesb.2013.04.034

Stein, M. and McElman, J.A. (1965), "Buckling of segments of toroidal shells", *AIAA J.*, **3**(9), 1704-1709. https://doi.org/10.2514/3.55185

Van Quyen, N., Van Thanh, N., Quan, T.Q. and Duc, N.D. (2021),

"Nonlinear forced vibration of sandwich cylindrical panel with negative Poisson's ratio auxetic honeycombs core and CNTRC face sheets", *Thin Wall. Struct.*, **162**, 107571. https://doi.org/10.1016/j.tws.2021.107571

Van Tien, N., Duc, V.M., Nam, V.H., Phuong, N.T., Ho, L.S., Dong, D.T., ... & Minh, T.Q. (2022), "Nonlinear postbuckling of auxetic-core sandwich toroidal shell segments with CNT-reinforced face sheets under external pressure", *Int. J. Struct. Stabil. Dyn.*, **22**(1), 2250006. https://doi.org/10.1142/S0219455422500067

Vuong, P.M. and Duc, N.D. (2019), "Nonlinear buckling and postbuckling of a FGM toroidal shell segment under a torsional load in a thermal environment within Reddy's third-order shear deformation shell theory", *Mech. Compos. Mater.*, **55**, 467-482. https://doi.org/10.1007/s11029-019-09826-9

Vuong, P.M. and Duc, N.D. (2020a), "Nonlinear static and dynamic stability of functionally graded toroidal shell segments under axial compression", *Thin Wall. Struct.*, **155**, 106973. https://doi.org/10.1016/j.tws.2020.106973

Vuong, P.M. and Duc, N.D. (2020b), "Nonlinear buckling and post-buckling behavior of shear deformable sandwich toroidal shell segments with functionally graded core subjected to axial compression and thermal loads", *Aerosp. Sci. Technol.*, **106**, 106084. https://doi.org/10.1016/j.ast.2020.106084

Wang, X. and Fu, T. (2024), "Improvement of broadband low-frequency sound insulation of sandwich plates with negative Poisson's ratio butterfly-shaped auxetic cellular", *Eng. Anal. Bound. Elem.*, **166**, 105852. https://doi.org/10.1016/j.enganabound.2024.105852

Yifeng, Z., Rong, L., Hien, P.L., Xiaoquan, L. and Yuxin, T. (2025), "Energy absorption characteristics of butterfly-shaped multi-cellular honeycomb structures under compressive loading", *Structures*, **75**, 108765. https://doi.org/10.1016/j.istruc.2025.108765

Yu, D., Kong, F. and Fu, T. (2024), "Sound transmission loss analysis of novel sandwich plate with star-shaped auxetic cellular cores," *Mech. Adv. Mater. Struct.*, 1-13. https://doi.org/10.1080/15376494.2024.2375029

Zhao, L.C., Xu, L. and Zeng, H.T. (2024), "Thermal buckling of temperature-dependent FG-CNT reinforced composite conical-conical joined shell using GDQ", *Thin Wall. Struct.*, **205**, 112320. https://doi.org/10.1016/j.tws.2024.112320

Zhao, S., Zhang, Y., Zhang, Y., Zhang, W., Yang, J. and Kitipornchai, S. (2022a), "Genetic programming-assisted micromechanical models of graphene origami-enabled metal metamaterials", *Acta Materialia*, **228**, 117791. https://doi.org/10.1016/j.actamat.2022.117791

Zhao, S., Zhang, Y., Zhang, Y., Yang, J. and Kitipornchai, S. (2022b), "Vibrational characteristics of functionally graded graphene origami-enabled auxetic metamaterial beams based on machine learning assisted models", *Aerosp. Sci. Technol.*, **130**, 107906. https://doi.org/10.1016/j.ast.2022.107906

Zhao, S., Zhang, Y., Wu, H., Zhang, Y. and Yang, J. (2022c), "Functionally graded graphene origami-enabled auxetic metamaterial beams with tunable buckling and postbuckling resistance", *Eng. Struct.*, **268**, 114763. https://doi.org/10.1016/j.engstruct.2022.114763